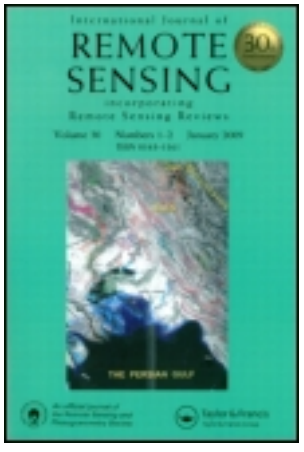

International Journal of Remote Sensing
Publication details, including instructions for authors and subscription information:
http://www.tandfonline.com/loi/tres20

Study of vertically resolved aerosol properties over an urban background site in Madrid (Spain)

F. Molero[a], F.J. Andrey[b], A.J. Fernandez[a], M.C. Parrondo[b], M. Pujadas[a], C. Córdoba-Jabonero[b], M.A. Revuelta[a] & F.J. Gomez-Moreno[a]

[a] Centro de Investigaciones Energéticas, Medioambientales y Tecnológicas (CIEMAT), Avda.Complutense, 40, Madrid 28040, Spain

[b] Instituto Nacional de Técnica Aeroespacial (INTA), Atmospheric Research and Instrumentation Branch, Torrejón de Ardoz, Madrid 28850, Spain

Published online: 11 Mar 2014.

To cite this article: F. Molero, F.J. Andrey, A.J. Fernandez, M.C. Parrondo, M. Pujadas, C. Córdoba-Jabonero, M.A. Revuelta & F.J. Gomez-Moreno (2014) Study of vertically resolved aerosol properties over an urban background site in Madrid (Spain), International Journal of Remote Sensing, 35:6, 2311-2326

To link to this article: http://dx.doi.org/10.1080/01431161.2014.894664

International Journal of Remote Sensing, 2014
Vol. 35, No. 6, 2311–2326, http://dx.doi.org/10.1080/01431161.2014.894664

Taylor & Francis
Taylor & Francis Group

Study of vertically resolved aerosol properties over an urban background site in Madrid (Spain)

F. Molero[a]*, F.J. Andrey[b], A.J. Fernandez[a], M.C. Parrondo[b], M. Pujadas[a], C. Córdoba-Jabonero[b], M.A. Revuelta[a], and F.J. Gomez-Moreno[a]

[a]*Centro de Investigaciones Energéticas, Medioambientales y Tecnológicas (CIEMAT), Avda. Complutense, 40, Madrid 28040, Spain;* [b]*Instituto Nacional de Técnica Aeroespacial (INTA), Atmospheric Research and Instrumentation Branch, Torrejón de Ardoz, Madrid 28850, Spain*

(*Received 13 September 2013; accepted 27 January 2014*)

This work presents a comparison of aerosol properties measured by *in situ* and remote-sensing instrumentation over an urban background site in Madrid (Spain) in autumn 2010. Aerosol size distribution was characterized at ground level by the combined use of two instruments and also in elevated layers by airborne *in situ* instrumentation. Simultaneously, vertically resolved lidar profiles provided information about the optical properties of aerosols present in the different layers observed. Backscatter-derived Ångström exponent, calculated using Mie theory with volume size distribution detected experimentally, yielded values lower than 0.5 near ground level, increasing to over 1.5 in elevated layers. The same trend was observed for values obtained using the lidar system. Size distribution measured at elevated layers indicated that the large exponents observed there are associated with size distribution, with a negligible contribution of coarse particles. The results are compromised by the major uncertainty associated with the backscatter-derived Ångström exponents, due to the low aerosol load detected in the elevated layers.

1. Introduction

Atmospheric aerosols have a significant impact on the radiative energy budget of the Earth–atmosphere system due to the direct effect from scattering and absorption of direct solar radiation, and indirectly by acting as condensation nuclei influencing cloud microphysics. The high variability of tropospheric aerosols in both space and time, together with the lack of long-term observations of aerosol properties, is one of the main reasons of the high level of uncertainty in regard to current radiative forcing estimates in studies of future climate change (Forster et al. 2007). Aerosol vertical distribution is of crucial importance in radiative transfer calculations (Deluisi et al. 1976). For instance, Johnson et al. (2008) demonstrated that the radiative effect of biomass-burning aerosol was sensitive to the vertical distribution of aerosol, concluding that interactions between different types of aerosol (biomass burning and dust) could cause absorption enhancements. In studying this vertical structure of the aerosol field and its temporal and spatial evolution, lidar (light detection and ranging) techniques represent a powerful tool because of their ability to provide aerosol profiles at high resolution in both time and the vertical dimension. Multi-wavelength lidars can provide additional information on aerosol microphysical properties due to the wavelength dependence of the backscatter and extinction coefficients (Müller et al. 2001). Systems with multiple wavelengths offer the opportunity

*Corresponding author. Email: f.molero@ciemat.es

to determine vertically resolved microphysical properties, such as size distribution parameters, volume concentrations, and refractive index (Böckmann et al. 2005). During the past decade, sophisticated inversion techniques have been developed successfully tested, permitting the retrieval of microphysical properties of aerosols from their optical properties provided by advanced multi-wavelength lidar observations. For aerosol sizes in the typical range of the accumulation mode, measurements of the backscatter and extinction coefficients at the Nd:YAG wavelength (1064, 532, and 355 nm) are necessary and sufficient to estimate aerosol volume and surface density, as well as the refractive index (Müller, Wandinger, and Ansmann 1999).

In this work, aerosol physical properties have been characterized using lidar and airborne and ground-based *in situ* instrumentation at an urban background site in Madrid (Spain). The main objective of this work is to compare the optical properties provided by lidar to those calculated using Mie theory, and the size distribution measured at ground level and in elevated layers. The height-resolved characterization provided by the airborne instrument allows a closure study of the backscatter-derived Ångström exponent in order to establish the reliability of this optical property. At ground level, aerosol size distribution (SD, hereafter) was continuously monitored between 15 nm and 20 μm diameter by means of a combination of a scanning mobility particle sizer and an optical particle counter. Additionally, airborne *in situ* measurements provided aerosol SD data between 0.10 and 3.0 μm in diameter using a passive cavity aerosol spectrometer probe (PCASP) installed onboard an INTA-C212 aircraft. Column-integrated characterization of the atmospheric aerosol was provided by a sun-tracking photometer.

This paper is organized as follows. Section 2 describes the field campaign, the experimental site, and the instrumentation and methodologies used in this study. Section 3 focuses on results and discussion, including a brief characterization of the prevailing synoptic situation on selected days, together with a comparison of vertically resolved measurements, explaining the synergy products obtained among them. Finally, Section 4 presents the main conclusions.

2. Instrumentation and methodology

2.1. Field campaign

Experimental data were taken during the Spain Lidar Intercomparison 2010 (SPALI10) field campaign in Madrid (40.45ºN, 3.73ºW, 663 m asl) from 18 October to 5 November 2010, as part of the quality assurance programme of EARLINET within the framework of the EARLINET-ASOS project (European Aerosol Research Lidar Network – Advanced Sustainable Observation System (http://www.earlinetasos.org)). The aim of the campaign was to compare simultaneous lidar measurements from several EARLINET network stations (Madrid, Granada, Barcelona and Evora) with a reference lidar system from Potenza, Italy, in order to assess their performance measuring the same atmosphere during the same time periods. The campaign allowed checking the performance of the systems and, when they were not fully satisfactory, the reasons for the failure were understood and the way to resolve them was defined (Freudenthaler, Amodeo, and Serikov 2011). The experimental site was the CIEMAT (Centro de Investigaciones Energéticas, Medioambientales y Tecnológicas) premises in the northwestern outskirts of the city, which can be considered an urban background site. The Madrid metropolitan area is located in the centre of the Iberian Peninsula, bordered to the north-northwest by a high mountain range (Sierra de Guadarrama) located 40 km away from the city, and to the

northeast and east by lower mountainous terrain. The population of the metropolitan area of Madrid is nearly 6 million, with a fleet of almost 3 million vehicles. Since its industrial activity is mainly light, the Madrid atmosphere is typically urban, fed by traffic emissions and also by domestic heating appliances in winter.

2.2. Instrumentation

2.2.1. Lidar system

The lidar system uses a pulsed Nd:YAG laser emitting at 1064, 532, and 355 nm, configured in a monostatic biaxial alignment pointing vertically to the zenith. The receiving line consists of a Newtonian telescope and wavelength separation unit with dichroic mirrors, interferential filters, and polarization cubes. The collected radiation is split into five channels allowing the detection of elastic signals at 1064, 532, and 355 nm and two Raman channels at 387 and 607 nm (nitrogen Raman-shifted signal from 355 and 532 nm, respectively). The optical set-up of the system yields a full overlap at about 300 m above the instrument. The lidar signal was registered in 1 min integrated time, with vertical resolution of 3.75 m.

2.2.2. Instrumented aircraft

A CASA C-212-200 aircraft, managed by the National Institute for Aerospace Technology (INTA) of Spain, carried airborne sensors to measure meteorological parameters and aerosol spectrometers to analyse aerosol particle SDs. This aircraft was designed as a light military transport aircraft and was modified for atmospheric research, with instruments fixed inside the aircraft cabin and at two solid points under the aircraft wings. During the SPALI10 campaign, measurements of temperature, dew point, pressure, GPS position, and aerosol SD were performed on 26 and 28 October 2010, at 02:00 and 08:00 UTC, respectively. On both days the airborne platform overflew the CIEMAT site, developing two vertical profiles following a spiral of about 4 km in diameter centred at a site approximately 0.9–3.7 km above sea level. A gentle ascent and descent rate of about 3.75 m s^{-1} was used in order to increase vertical resolution.

Aerosol particle SDs were provided by a passive cavity aerosol spectrometer probe, model 100X (PCASP-100X), manufactured by Particle Measuring Systems Inc (Boulder, CO, USA). The PCASP instrument is an optical particle counter (OPC) designed for sizing aerosols by illuminating particles and collecting the light scattered into a fixed solid angle. This system is based on a He:Ne laser source at 632.8 nm, and light scattered by the particles is collected and classified into one of 15 channels ranging from 0.1 to 3.0 μm in diameter (Fiebig et al. 2002). The relationship between scattering cross-section and particle diameter at the channel limits is dependent on the particle shape and refractive index, so this information is required in advance to interpret the optical particle counter data. If the refractive index of the sampled particles is different from the calibration particle refractive index, the channel limits are corrected by applying the Mie theory. PCASP partially dries the sample before it is sized on account of deceleration in the inlet cone, and due to focusing of the sample into the laser beam with dried sheath air. As a result of this drying process, the relative humidity of the sample is lower than 40% (Strapp, Leaitch, and Liu 1992). The measurement uncertainties associated with the PCASP have been discussed by several authors (i.e. Kim and Boatman 1990; Strapp,

Leaitch, and Liu 1992; Baumgardner et al. 2005), who reported the accuracy of size characterization and aerosol concentration as 16% and 20%, respectively.

2.2.3. *Ground-based* in situ *instrumentation*

At ground level, the temporal evolution of particle number and mass concentration for particles of aerodynamic diameter less than 10, 2.5, and 1 μm (PM10, PM2.5, and PM1, respectively) were monitored at the experimental site using an OPC model 1107, GRIMM Aerosol Technik, Ainring, Germany). Dry ambient sub-micrometer SDs were monitored at the site using a scanning mobility particle sizer (SMPS) (model 3936, TSI Inc., Shoreview, MN, USA), combining a long differential mobility analyser (DMA) and a condensation particle counter (CPC, model 3775, TSI Inc.) working in scanning mode. This particle spectrometer uses the relationship between particle mobility and diameter to calculate particle size (Knutson and Whitby 1975). Before entering the DMA, the sample is dried by a Nafion drier and particles are neutralized by a Kr-85 radioactive source. Once in the DMA, particles are classified according to their electrical mobility and then counted by the CPC. Data were obtained in the size range 0.015–0.661 μm by using rates of 0.3 and 3.0 l min^{-1} for aerosol and sheath flows, respectively. Datasets were also corrected for losses caused by diffusion processes within the instrument (Willeke and Baron 1993).

For larger particles, another OPC (model 1108, GRIMM Aerosol Technik) was used, providing particulate counts distributed among 15 channels (0.3, 0.4, 0.5, 0.65, 0.8, 1.0, 1.6, 2.0, 3.0, 4.0, 5.0, 7.5, 10, 15, and 20 μm diameter) by 90º laser light scattering. Ambient air, drawn into the unit, passes through a flat laser beam produced by a laser diode, and the scattered signals are detected by a multi-channel pulse height analyser for size classification (Grimm and Eatough 2009).

The GRIMM 1108 and SMPS diameter ranges overlap in the size range from 0.30 μm (lower end of the GRIMM) to 0.66 μm (upper end of the DMA). Therefore, it is possible to obtain a single plot for number distributions between 0.015 and 20 μm by combining the data from both instruments. Volume size distributions ($dV/d\ln(d)$) were calculated assuming that aerosol particles were spheres with a radius equal to the centre radius of each bin as measured by the instruments.

2.2.4. *CIMEL sun photometer*

Column-integrated characterization of the atmospheric aerosol was performed by means of the automatic sun-tracking photometer, CIMEL CE-318-4 (Holben et al. 1998), operated by Spanish Meteorological Agency personnel. This instrument makes direct sun irradiance measurements with a 1.2º full field of view every 15 min at 340, 380, 440, 670, 870, 940, and 1020 nm. It requires about 8 s to scan all seven wavelengths, with a motor-driven filter wheel positioning each filter in front of the detector. These solar extinction measurements are then used to compute aerosol optical depth (AOD) at each wavelength except for the 940 nm channel, which is used to retrieve total column water vapour.

2.2.5. *Backward trajectories*

The HYSPLIT.4 (Hybrid Single Particle Lagrangian Integrated Trajectory) model developed by the NOAA (National Oceanic and Atmospheric Administration) Air Resources Laboratory (ARL) (Draxler and Rolph 2003) was used to calculate 5-day backward

trajectories of air masses reaching Madrid at six different altitudes above ground level (500, 1000, 2000, 3000, 4000, and 5000 m agl), by means of the vertical wind component. This model uses the Global Data Analysis System meteorological files as data input, with a spatial resolution of 1º × 1º every 3 hours generated and maintained by ARL (Draxler et al. 2009).

2.3. Methodology

2.3.1. Lidar-derived products

From the elastic lidar signal, aerosol backscatter coefficient profiles were retrieved using the Klett–Fernald–Sasano algorithm (Klett 1981; Fernald 1984; Sasano and Nakane 1984). Radio-sounding launches were performed during the entire campaign period for each measurement session. Temperature and pressure profiles provided by radiosonde data were used to calculate molecular profiles. Lidar signals can be fitted to these calculated 'Rayleigh' profiles to choose the aerosol-free vertical range for the reference value required by the inversion algorithm The retrieval of backscatter coefficient profiles requires the use of an *a priori* selected value for the lidar ratio (i.e. the ratio between aerosol extinction and backscatter coefficient). During daytime measurements, a synergetic approach with Sun-photometer data was used to select an appropriated lidar ratio value (Takamura, Sasano, and Hayasaka 1994). The approach consisted of computing lidar profiles of extinction coefficient, using different values of lidar ratio as input, and comparing the AOD obtained by integrating the extinction coefficient profile with that provided by the Sun photometer, converted to the lidar wavelengths from CIMEL's closest ones by means of the Ångström relation:

$$\overset{o}{a} = -\log[\mathrm{AOD}(\lambda_1)/\mathrm{AOD}(\lambda_2)]/\log(\lambda_1/\lambda_2), \tag{1}$$

where å is the Ångström exponent and AOD is aerosol optical depth, obtained at wavelengths λ_1 and λ_2.

As the biaxial lidar system does not provide information in the near range due to overlap limitations between the laser beam and the telescope field of view, the backscatter coefficient value in this near range was assumed constant and equal to the first reliable value found at the lowest full-overlap height (~300 m agl). A lidar ratio value was selected when the difference between lidar- and CIMEL-derived AOD was minimized. It is important to highlight that this approach assumes an atmosphere with constant aerosol lidar ratio along the entire column. If different types of aerosol, with different lidar ratio values, were present in elevated layers, the approach would provide an averaged lidar ratio between the lidar ratio of the aerosols in the mixed layer and that of aerosols in elevated layers.

As mentioned in Section 1, multi-wavelength lidars can provide additional information on aerosol microphysical properties due to the wavelength dependence of the backscatter and extinction coefficients. One parameter that provides such information is the backscatter-derived Ångström exponent (BAE). This parameter is obtained by applying the same equation as the usual Ångström exponent mentioned above (see Equation (1)), but using the backscatter coefficient $\beta(\lambda, z)$ as a function of wavelength λ and altitude z, rather than the AOD:

$$\mathrm{BAE}(z) = -\log[\beta(\lambda_1, z)/\beta(\lambda_2, z)]/\log(\lambda_1/\lambda_2). \tag{2}$$

This change allows a vertically resolved optical parameter to be obtained. On the other hand, the backscatter coefficient rather than the extinction coefficient is employed because the former is considered to be a more reliable lidar-derived product. Employing one or other coefficient will be equivalent only in the case where the same lidar ratio has been used in the inversion of the two channels. In this work, BAE between the 532 and 355 nm wavelengths and 1064 and 532 nm wavelengths is calculated. Different values of this parameter indicate different aerosol characteristics.

2.3.2. Mie calculations

Aerosol optical properties, such as backscatter coefficient and BAE parameter, can be calculated by applying the Mie theory (Bohren and Huffman 1983) to aerosols of known SD, refractive indices, and incident light wavelength. Thus the aerosol backscatter coefficient as a function of altitude z and wavelength λ is given by

$$\beta(z,\lambda) = \int_{d_{\min}}^{d_{\max}} \left(\frac{\pi d}{2}\right)^2 Q_{\mathrm{b}}(m, \pi d/\lambda) \sum \frac{\mathrm{d}N(d,z)}{\mathrm{d}\ln(d)} \mathrm{d}\ln(d), \tag{3}$$

where d is the Stokes diameter of the particle; Q_{b} is the backscattering efficiency, computed by means of the Mie theory (Matzler 2002); m is the complex refractive index of aerosol particles; and $\sum \mathrm{d}N(d,z)/\mathrm{d}\ln(d)$ is the sum of lognormal particle numerical distributions found at altitude z, each expressed as follows:

$$\frac{\mathrm{d}N(d,z)}{\mathrm{d}\ln(d)} = \frac{A}{\sqrt{2\pi}\ln\sigma_g} \exp\left\{-\frac{1}{2}\left(\frac{\ln\left(d/d_{\mathrm{g}}\right)}{\ln\sigma_{\mathrm{g}}}\right)^2\right\}, \tag{4}$$

where A is the total aerosol number concentration; d is the particle diameter; d_{g} is the geometric mean diameter; and σ_{g} is the geometric standard deviation for the aerosol mode.

It will be noted that the integral in Equation (3) refers to the logarithmically spaced size ranges, because the aerosol numerical lognormal distribution is expressed in such a manner. Once the backscatter coefficient is calculated for the three lidar wavelengths, the BAE at each two pairs of lidar wavelengths can be calculated using Equation (2). When aerosol numerical distributions are available at different altitudes, such as those provided by the airborne PCASP instrument, BAE can be calculated for each height in order to compare them with the vertically resolved BAE profiles provided by the multi-wavelength lidar system. The errors associated with the Mie calculated values are derived by error propagation, assuming no uncertainty in wavelength value, an estimated uncertainty of 10% in the refractive index value (Osterloh et al. 2009), and the uncertainty derived by the least mean squared fit of the SD to lognormal distributions. The application of Mie theory may be an additional source of error when the non-sphericity of particles is relevant. However, the particles found in this work were of small size and the assumption of spheres is plausible.

3. Results and discussion

3.1. Synoptic situation

Meteorological analysis of the study period has shown a synoptic situation mainly governed by high-pressure systems over the Iberian Peninsula, except for the last three days of October. Between 18 and 24 October, the high-pressure system (1021 hPa), or sometimes a barometric swamp, blocked the entry of air masses from the Atlantic and promoted stagnation, reducing the ventilation of the atmosphere at the study site. The pressure gradient at the surface was very low and consequently there was an absence of wind, with clear and dry conditions. Analysis of the backward trajectories provided by the HYSPLIT model (not shown) indicated low circulation and recirculation at lower levels, with some Atlantic influence at higher altitudes. Temperature near the surface varied from 10ºC to 20ºC and relative humidity from 10% to 60%. On 24 October, the air mass changed due to the influence of one high-pressure system over the Azores and another over the British Isles. The Azores high-pressure system extended towards the Iberian Peninsula on subsequent days, again producing a barometric swamp, although with the presence of mid-altitude clouds between 26 and 29 October. Following this, there were 3 days of rain, from 29 to 31 October, produced by the arrival of a cold front from the Atlantic and which led to a wash-out of the atmosphere over Madrid after the previous period of stagnation. At the beginning of November, the Azores high-pressure system and a low-pressure system over the Mediterranean were causing the ingress of air masses from the Atlantic. Pressure gradients and winds were higher than in the previous period, with a slight increase in surface pressure from 1 to 4 November. Temperatures at the surface ranged from 10ºC to 22ºC and relative humidity from 45% to nearly 100%. The backward trajectories from HYSPLIT indicated Atlantic provenance with no mixing between levels.

3.2. Temporal evolution of mass concentration and AOD

The temporal evolution of PM_{10}, $PM_{2.5}$, and PM_1 mass concentration at ground level is shown in the lower panel of Figure 1. Local pollution produced events during the morning traffic rush-hour – between 7:00 and 9:00 local time – or later until midday, due either to the formation of secondary pollutants or transport processes. These events are clearly identified by sharp peaks of PM_{10}. $PM_{2.5}$ and PM_1 show a similar trend, but less pronounced. Between these pollution peaks, the background pollution levels increased from day to day from 18 to 24 and from 25 to 29 October due to stagnation of the air mass. On 24 October, the sudden decrease in particle concentration was due to the above-mentioned change in air mass over the site. On the other hand, the synoptic situation from 31 October to 5 November allowed clearing of the atmosphere from day to day, with lower PM_{10}, $PM_{2.5}$, and PM_1 mass concentration compared to levels before the rain episode, due to the inflow of Atlantic air masses that prevented the accumulation of pollution that had arisen over the preceding days. The temporal evolution of AOD provided by the sun photometer is shown in the upper panel of Figure 1, for wavelengths closest to the lidar ones. Error bars, established by the instrument accuracy parameters, are illustrated in the legend for clarity. The evolution resembled the above-mentioned situation, with AOD increasing from 0.02 to 0.15 at 500 nm between 19 and 24 October. On most days of the second week (25–29 October), CIMEL measurements were hindered by the presence of cloud. In the final week (1–4 November), AOD at 500 nm was lower, ranging from 0.01 to 0.08, due to the influence of clean air masses from the Atlantic. The open symbols in Figure 1 (top panel) refer to lidar-derived AOD values, obtained by

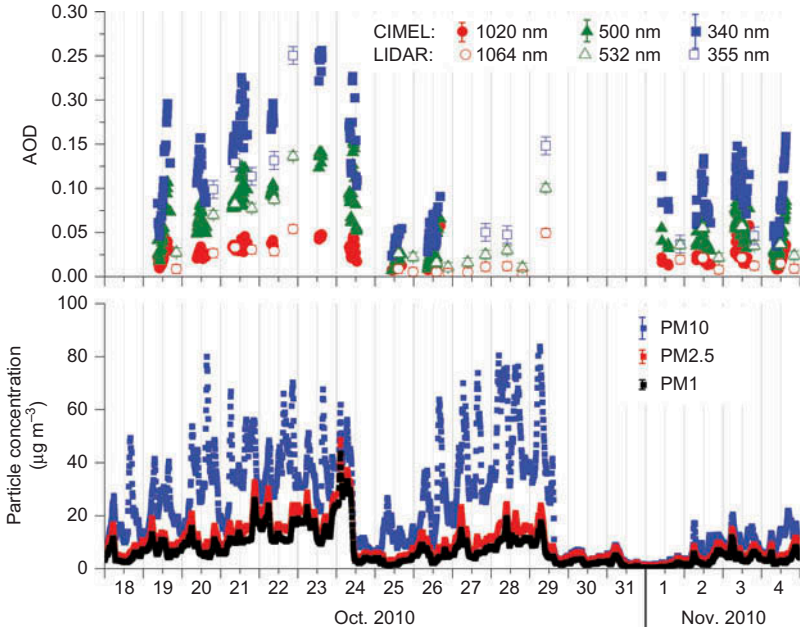

Figure 1. Temporal evolution from 18 October to 4 November of: (upper panel) CIMEL-derived AOD (filled symbols) and lidar-derived AOD (open symbols) and (lower panel) particle mass concentration at size ranges PM_{10}, $PM_{2.5}$, and PM_1 at ground level.

integrating the aerosol extinction coefficient profiles produced by the Klett–Fernald–Sasano algorithm between ground level and 5 km agl. Error bars are calculated for each point by error propagation of the extinction coefficient profiles' errors. Each profile was visually inspected to ascertain that no aerosol was present over 5 km agl. On some occasions, cirrus clouds were present to about 10 km agl but their AOD, obtained from the difference in the molecular signal fitted to the lidar range-corrected signal before and after cloud appearance, were negligible compared with total column AOD. As mentioned in Section 2.3.1, the lidar ratio was selected to match the AOD provided by the CIMEL. Two days were selected to perform this calculation: 21 October, when the values obtained were LR(355 nm) = 87 ± 17 sr, LR(532 nm) = 57 ± 16 sr, LR(1064 nm) = 53 ± 14 sr; and 2 November, when LR(355 nm) = 70 ± 23 sr, LR(532 nm) = 70 ± 21 sr, and LR (1064 nm) = 70 ± 23 sr were recorded. As will be seen from Figure 1, the measurements coincide with the days when the lidar ratio was calculated. The other days presented problems in performing reliable computing, such as very low AOD values or the presence of cirrus clouds. The lidar ratios obtained on 21 October were used in the Klett–Fernald–Sasano algorithm for data between 18 and 29 October, and those obtained on 2 November for data between 1 and 4 November. The reason for selecting these values is based on the aerosol characteristics found at ground level over the site. Between 18 and 29 October, stagnation of the air mass allowed ageing of the aerosol, including secondary aerosol formation and probable growth. On the other hand, from 1 November onwards, the air mass changed from day to day so only fresh, locally produced primary aerosols were present. This difference in aerosol characteristics seems also to have affected the lidar ratio and its variability with wavelength, although further study incorporating more cases

is required. As will be observed in the upper panel of Figure 1, reasonable agreement is found between CIMEL- and lidar-derived AOD.

3.3. *Comparison of ground-level and airborne* in situ *measurements*

Figure 2 shows the lidar 'quicklook' for the 25 October night-time session. The 'quicklook' at 1064 nm was selected because this wavelength is less influenced by molecular contribution. Figure 2 shows a mixed layer up to 1.5 km asl, with several layers aloft. These layers are barely seen in the backscatter coefficient profiles (see Figure 3, left panel), with only the one located between 2.3 and 2.8 km asl distinguishable from noise. This indicated the low aerosol concentration present in this layer, and also pointed out the difficulties involved in correctly characterizing the aerosol properties with lidar, where the relevant features of the profiles can be hidden by noise. This layer is also observable on the airborne PCASP profile (black and grey lines in Figure 3, left panel) plotted for channel 4, corresponding to a particle of diameter 0.194 μm located in the centre of the fine mode. The layer appears at a slightly lower altitude (2.2–2.4 km asl), probably due to temporal displacement between the measurements (00:30–01:00 UTC for the lidar system and 02:15–02:50 UTC for the PCASP instrument) imposed for safety reasons by the aircraft crew. Such decreases in the higher layer altitude will be observed on the quicklook, but they remain at the same height between the aircraft upward spiral (02:15–02:31 UTC, black line) and downward spiral (02:31–02:50 UTC, grey line). The BAE of both the mixed layer and this elevated layer are plotted on the right-hand panel of Figure 3, with low values (around 0.5 and 1.5 m^{-1} sr^{-1} for the 532–355 and 1064–532 nm wavelengths pairs, respectively) indicating the presence of large particles near ground. On the other hand, aerosols present in the layer aloft were presumably rather small, as they produced larger BAE values (around 2.3 and 2.6 for the 532–355 and 1064–532 nm

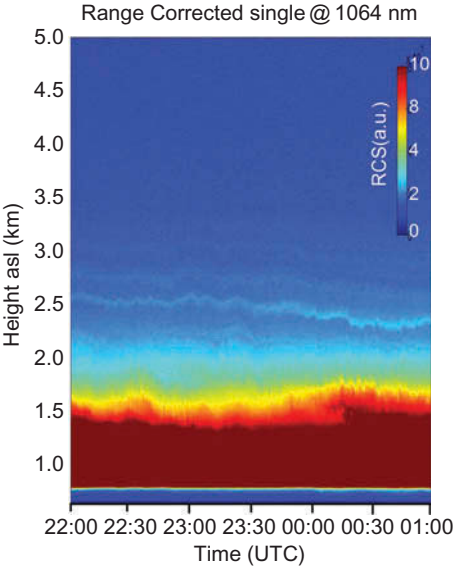

Figure 2. 'Quicklook' produced as colour-coded plots of the range-corrected 1064 nm lidar signals *versus* time and height from surfaces up to 5 km asl for the measurement session between 25 October at 22:00 UTC and 26 October at 01:00 UTC.

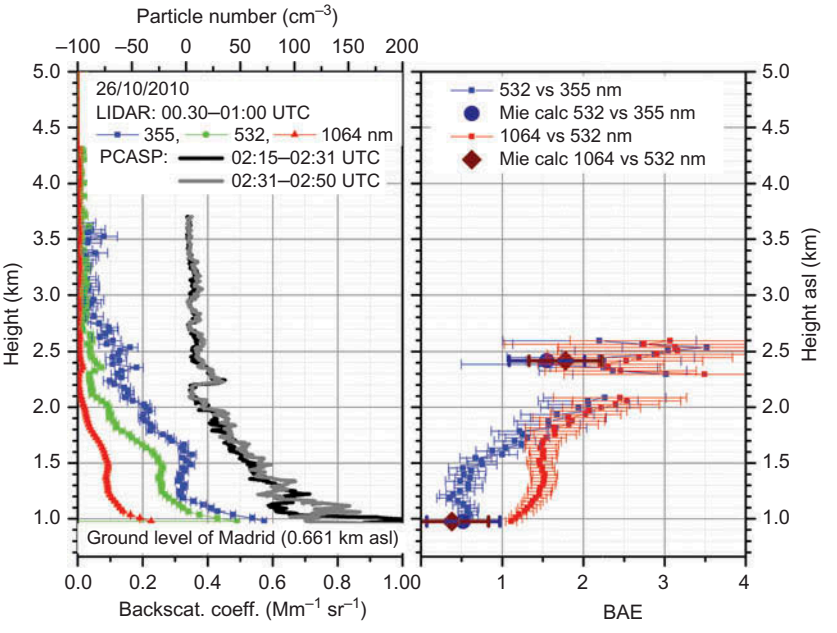

Figure 3. Left panel: vertically resolved aerosol backscatter coefficient profiles obtained by averaging signals between 00:30 and 01:00 UTC, and also the particle number profile provided by the PCASP instrument (black line for aircraft upward spiral and grey for downward spiral, shifted for clarity; note top axis displacement) between 02:15 and 02:50 UTC. Right panel: BAE calculated between 532 and 355 nm (blue symbols) and between 1064 and 532 nm (red symbols) wavelength pairs. Results from the Mie theoretical calculations are also shown (filled symbols).

wavelengths pairs, respectively). In the same graph, the values obtained by Mie computing were plotted as full symbols. These values were calculated using the refractive index provided by the CIMEL instrument and the numerical distributions measured by PCASP at those altitudes, as explained in Section 2.3.1. As mentioned in that section, the accuracy of the refractive index cannot be guaranteed due to the low AOD values. Also, the SD provided by the PCASP instrument, limited to a maximal particle diameter of 3 μm, can introduce inaccuracies in the computation, as be further explained below. Despite these limitations, the computed BAE values agreed reasonably well with the experimental ones.

Figure 4 shows aerosol volume SD vs. diameter between 0.01 and 100 μm, in logarithmic scale, obtained on 26 October between 02:00 and 03:00 UTC. Four different volume SDs are plotted, first that obtained at ground level by the combination of the SMPS and GRIMM instruments averaged over one hour; secondly that provided by the airborne PCASP instrument at the lowest altitude reached by the aircraft (lowest layer (LL in graph): 0.94 km asl, averaged over 40 m vertically, corresponding to 45 s); thirdly that obtained by averaging the whole mixed layer (ML: 0.94–2 km asl, averaged over 6 min); and finally, that obtained by averaging the elevated layer (EL: 2.23–2.35 km asl, averaged over 65 s). Several features in Figure 4 can be highlighted: first, the SD observed at ground level was bimodal, with the first mode (fine mode) with diameter between <0.015 and 1 μm, and a second mode (coarse mode) with diameter between 1 and >20 μm. Between these modal values, there was a minimum (inflection point) corresponding to a diameter of about 1 μm. Secondly, the three instruments (SMPS, GRIMM, and PCASP)

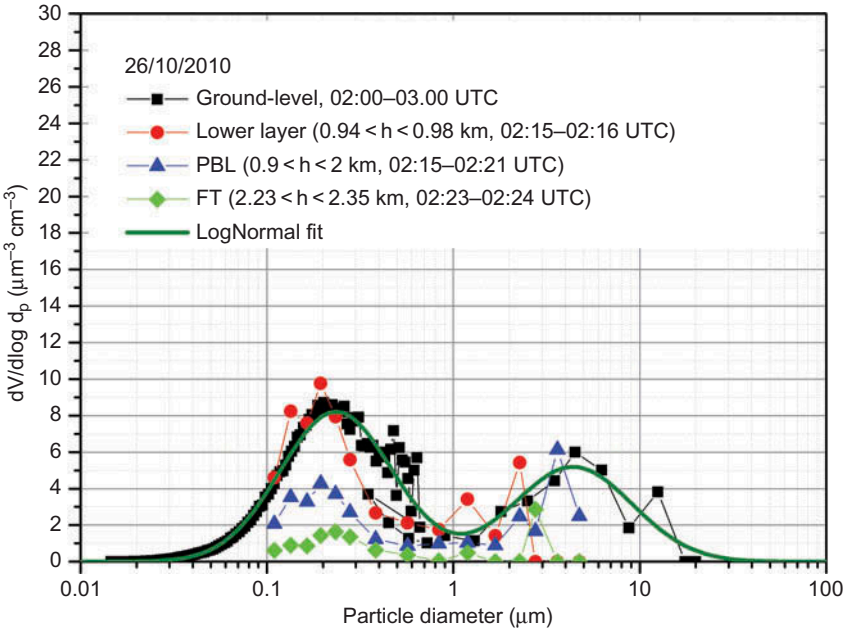

Figure 4. Volume SD measured at ground level by the combined SMPS + GRIMM instruments and that obtained at different altitudes by airborne PCASP on 26 October between 02:00 and 03:00 UTC.

presented problems in properly characterizing particles in their widest range of channels. For the SMPS instrument, those channels corresponded to a diameter between 0.3 and 0.6 μm, where increasing noise can be seen. This limitation was partially corrected by the overlap range with the GRIMM instrument. On the other hand, this latter instrument presented problems in determining particles larger than 8 μm. And finally, characterization of the coarse mode by PCASP suffered from this limitation, in this case for particles of diameter over 1 μm. This limitation might have affected computation of BAE values by the Mie theory, as mentioned above. As will be observed from Figure 4, agreement between the lowest layer SD provided by PCASP and the ground-level distribution provided by the SMPS + GRIMM combination was adequate, although PCASP SD was slightly narrower in area of the fine mode with larger diameters. The EL SD presented roughly the same SD but with reduced values.

A second flight was conducted by the INTA aircraft on 28 October, between 08:21 and 08:54 UTC under daytime conditions. This relaxed the safety requirements of the aircraft crew, allowing a better temporal coincidence between measurements. Figure 5 shows the quicklook, and Figure 6 the vertically resolved optical profiles provided by the lidar in this case. The black line on the quicklook represents aircraft altitude. It will be noted that the mixed layer reached 1.8 km asl, with one layer aloft located between 2.11 and 2.15 km asl. This latter layer was also observable on the airborne PCASP profile (black and grey lines in the middle panel). The aloft layer, and also the top of the mixed-layer altitude, changed between the aircraft upward spiral (08:21–08:37 UTC, black line) and the downward spiral (08:37–08:54 UTC, grey line). by roughly 60 m. This variation could not be taken into account in the lidar data processing, as at least 30 min must be averaged to achieve adequate signal-to-noise ratio for the data inversion.

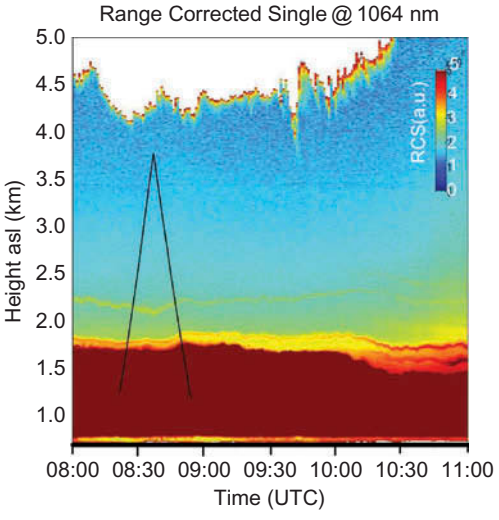

Figure 5. As Figure 2 but on 28 October between 08:00 and 11:00 UTC.

The BAE for the mixed layer indicates again the presence of large particles, due to the low values (around 0.5 and 1.1 for the 532–355 and 1064–532 nm wavelength pairs, respectively). The aerosols present in the layer aloft must be very small, as they produced rather high BAE values (around 2.8 and 2.6 for the 532–355 and 1064–532 nm

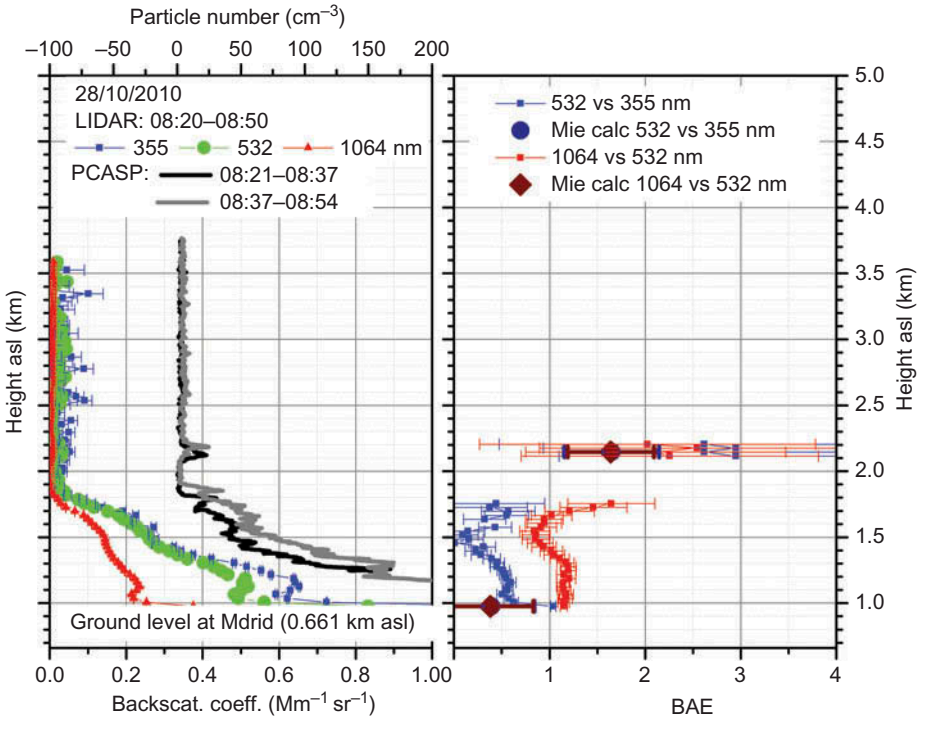

Figure 6. As Figure 3 but on 28 October between 08:00 and 11:00 UTC.

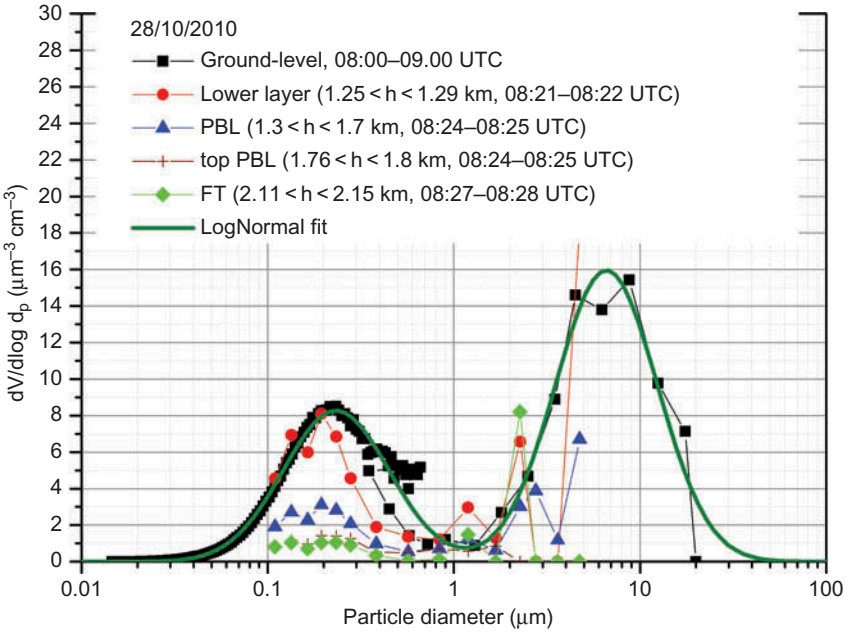

Figure 7. As Figure 4 but on 28 October between 08:00 and 9:00 UTC.

wavelength pairs, respectively). The values obtained by Mie computing, plotted as full symbols in Figure 6, yield lower values (0.4 for the mixed layer and 1.68 for the EL for both wavelengths pairs) than the lidar system, which may be explained by the limitation in the refractive index and SD values mentioned above.

Figure 7 shows aerosol volume SD *versus* diameter between 0.01 and 100 µm, in logarithmic scale, obtained on 28 October between 08:00 and 09:00 UTC. The same four different volume SDs are plotted as in Figure 4, with the lowest altitude layer (LL) now located at a slightly higher altitude (1.25 km asl, averaged over 40 m), the mixed layer (ML) from 1.25 to 1.7 km asl, and the elevated layer (EL) from 2.11 to 2.15 km asl. The fine and coarse mode at ground level and the fine mode for the elevated layer were fitted using lognormal distribution, plotted as lines in Figures 4 and 7. The parameters obtained are shown in Table 1.

Table 1. Lognormal parameters, explained in Equation (4), calculated by fitting ground-level SD as measured by combined SMPS + GRIMM instruments and the aloft layer SD measured by the airborne PCASP instrument.

Date	Layer	Height (km asl)	Mode	A (µm^3 cm^{-3})	d_g (µm)	lnσ_g
26 October	Ground	0.661	Fine	13.2 ± 0.15	0.223 ± 0.002	0.624 ± 0.007
26 October	Ground	0.661	Coarse	9.5 ± 1.2	4.4 ± 0.5	0.7 ± 0.1
26 October	Aloft	2.23–2.35	Fine	2 ± 0.3	0.235 ± 0.001	0.5 ± 0.1
28 October	Ground	0.661	Fine	12.65 ± 0.07	0.222 ± 0.001	0.604 ± 0.003
28 October	Ground	0.661	Coarse	25 ± 2	6.6 ± 0.4	0.64 ± 0.05
28 October	Aloft	2.11–2.15	Fine	1.5 ± 0.2	0.19 ± 0.01	0.5 ± 0.1

The bimodal distribution was obtained again, with roughly the same values of the median diameter for the fitted lognormal functions for the fine mode, but displaced by 2.2 μm for the coarse one, as will be seen in Table 1. Also the A parameter increased almost twofold due to the higher load of coarse aerosols. Agreement between the lowest layer SD provided by the PCASP and the ground-level distribution provided by the SMPS + GRIMM combination was adequate (Molero et al. 2012).

4. Conclusion

A field campaign was carried out at an urban background site in Madrid to study the optical and microphysical properties of aerosol particles on a vertical scale ranging from ground level to elevated layers. The vertically resolved aerosol optical properties provided by a multi-wavelength lidar system at three elastic wavelengths, complemented by the CIMEL-derived AOD to select appropriate lidar ratios, provided information about the type of aerosol present in the different layers observed. The comparison of lidar- and CIMEL-derived AOD yielded good agreement, even in those cases where the lidar ratio was inferred from other measurement sessions due to low AOD values or the presence of cirrus clouds. The refractive indices provided by the CIMEL instrument were employed in the correction of the PCASP size distribution size channels, and also in the computation of optical properties by Mie theory. The low AOD values detected during the campaign, which reduced the accuracy of the calculated refractive indices, might have compromised these results. The comparison of size distribution measured by ground level and airborne *in situ* instruments yielded adequate agreement for the lowest layer (940 and 1250 m asl on 26 and 28 October, respectively) for the fine mode of the bimodal shape usually obtained. A typical urban fine aerosol mode centred ~0.20 μm was found at the four levels studied (ground level, LL, ML, and EL), with concentrations which appeared to decrease with height above the LL. Furthermore, the theoretical computation of the backscatter-derived Ångström exponent using Mie theory with size distribution detected at elevated layers resembled the results obtained with the lidar system, although with slightly lower values. This allows the conclusion that the large backscatter-derived Ångström exponent observed at elevated layers detected by the lidar system may have been caused by size distribution with a negligible contribution from coarse particles. Despite the fact that the elevated layers detected during the campaign had a low aerosol load, the synergy of the suite of instruments employed allowed characterization of several of their properties. Further investigations are required to relate those properties to other vertically resolved aerosol optical and microphysical properties that could be obtained with multi-wavelength lidar systems

Acknowledgements

The work was supported by the European Union under the EARLINET-ASOS project (contract no. 025991 (RICA)) and by MICINN (Spanish Ministry of Science and Innovation) through projects CGL2010-17777 (PHAESIAN), CGL2010-09225-E (ISLIDAR), and CGL2010-10012-E (MISPA-LIDAR). The authors gratefully acknowledge the AEMET for the provision of the CIMEL data within the framework of collaboration agreement 10/161. The authors are grateful to INTA Aerial platforms of the Spanish ICTS programme, and the Spanish Air Force, via the CLAEX unit, for their efforts in maintaining and operating the aircraft. The authors gratefully acknowledge the NOAA Air Resources Laboratory (ARL) for the provision of the HYSPLIT transport and dispersion model.

References

Baumgardner, D., G. B. Raga, J. C. Jimenez, and K. Bower. 2005. "Aerosol Particles in the Mexican East Pacific Part I: Processing and Vertical Redistribution by Clouds, Atmos." *Chemical Physics* 5: 3081–3091. doi:10.5194/acp-5-3081-2005.

Bohren, C. F., and D. R. Huffman. 1983. *Absorption and Scattering of Light by Small Particles*. Hoboken, NJ: John Wiley.

Böckmann, C., I. Mironova, D. Müller, L. Schneidenbach, and R. Nessler. 2005. "Microphysical Aerosol Parameters from Multiwavelength Lidar." *Journal of the Optical Society of America A* 22: 518–528. doi:10.1364/JOSAA.22.000518.

Deluisi, J., P. M. Furukawa, D. A. Gillette, B. G. Schuster, R. J. Charlson, W. M. Porch, R. W. Fegley, B. M. Herman, R. A. Rabinoff, J. T. Twitty, and J. A. Weinman. 1976. "Results of a Comprehensive Atmospheric Aerosol-Radiation Experiment in the Southwestern United States Part I: Size Distribution, Extinction Optical Depth and Vertical Profiles of Aerosols Suspended in the Atmosphere." *Journal of Applied Meteorology* 15: 441–454. doi:10.1175/1520-0450(1976)015<0441:ROACAA>2.0.CO;2.

Draxler, R. R., and G. D. Rolph. 2003. *HYSPLIT* (*HYbrid Single- Particle Lagrangian Integrated Trajectory*). Silver Spring, MD: NOAA Air Resources Lab. Model access via NOAA ARL READY Website http://www.arl.noaa.gov/ready/hysplit4.html

Draxler, R. R., B. Stunder, G. Rolph, and A. Taylor. 2009. *Hysplit 4 User's Guide*. Silver Spring, MD: NOAA Air Resources Laboratory.

Fernald, F. G. 1984. "Analysis of Atmospheric Lidar Observations: Some Comments." *Appllied Optics* 23: 652–653. doi:10.1364/AO.23.000652.

Fiebig, M., A. Petzold, U. Wandinger, M. Wendisch, C. Kiemle, A. Stifter, M. Ebert, T. Rother, and U. Leiterer. 2002. "Optical Closure for an Aerosol Column: Method, Accuracy, and Inferable Properties Applied to a Biomass-Burning Aerosol and its Radiative Forcing." *Journal of Geophysics Research* 107 (D21): 8130. doi:10.1029/2000JD000192.

Forster, P., V. Ramaswamy, P. Artaxo, T. Berntsen, R. Betts, D. W. Fahey, J. Haywood, J. Lean, D. C. Lowe, G. Myhre, J. Nganga, R. Prinn, G. Raga, M. Schulz, and R. Van Dorland. 2007. "Changes in Atmospheric Constituents and in Radiative Forcing." In *Climate Change 2007: The Physical Science Basis*, *Contribution of Working Group I to the Fourth Assessment Report of IPCC*, edited by S. Solomon, 129–234. Cambridge: Cambridge University Press.

Freudenthaler, V., A. Amodeo, and I. Serikov. 2011. *Report on IC-campaign*, *Part 1 + 2 Deliverable D3.6*, *EARLINET-ASOS: European Aerosol Research Lidar Network –Advanced Sustainable Observation System Project Internal Report No. 25991*. March. Accessed November 27, 2013. http://www.earlinet.org/

Grimm, H., and D. J. Eatough. 2009. "Aerosol Measurement: The Use of Optical Light Scattering for the Determination of Particulate Size Distribution, and Particulate Mass, Including the Semi-Volatile Fraction." *Journal of the Air & Waste Management Association* 59: 101–107. doi:10.3155/1047-3289.59.1.101.

Holben, B. N., T. F. Eck, I. Slutsker, D. Tanré, J. P. Buis, A. Setzer, E. Vermote, J. A. Reagan, Y. J. Kaufman, T. Nakajima, F. Lavenu, I. Jankowiak, and A. Smirnov. 1998. "AERONET – A Federated Instrument Network and Data Archive for Aerosol Characterization." *Remote Sensing of Environment* 66: 1–16. doi:10.1016/S0034-4257(98)00031-5.

Johnson, B. T., B. Heese, S. A. McFarlane, P. Chazette, A. Jones, and N. Bellouin. 2008. "Vertical Distribution and Radiative Effects of Mineral Dust and Biomass Burning Aerosol Over West Africa During DABEX." *Journal of Geophysics Research* 113: D00C12. doi:10.1029/2008JD009848.

Kim, Y. J., and J. F. Boatman. 1990. "Size Calibration Corrections for the Active Scattering Aerosol Spectrometer Probe (ASASP-100x)." *Aerosol Science and Technology* 12: 665–672. doi:10.1080/02786829008959381.

Klett, J. D. 1981. "Stable Analytical Inversion Solution for Processing Lidar Returns." *Applied Optics* 20: 211–220. doi:10.1364/AO.20.000211.

Knutson, E. O., and K. T. Whitby. 1975. "Aerosol Classification by Electric Mobility: Apparatus Theory and Applications." *Journal of Aerosol Science* 6: 443–451. doi:10.1016/0021-8502(75)90060-9.

Matzler, C. 2002. *MATLAB Functions for Mie Scattering and Absorption* (vol. 2002–11). Research Report. Bern: Institut für Angewandte Physik, University of Bern.

Molero, F., M. Sicard, F. Navas-Guzmán, J. Preißler, A. Amodeo, V. Freudenthaler, A. J. Fernandez, S. Tomas, M. J. Granados, F. Wagner, A. Giunta, I. Mattis, M. Pujadas, A. Comeron, L. Alados-Arboledas, J. L. Guerrero-Rascado, G. D'Amico, D. Lange, J. A. Bravo-Aranda, D. Kumar, G. Pappalardo, J. Giner, C. Muñoz, and F. Rocadenbosch. 2012. "Study on Aerosol Properties over Madrid (Spain) by Multiple Instrumentation during SPALI10 Lidar Campaign." *Optica Pura Y Aplicada* 45 (4): 405–413. doi:10.7149/OPA.45.4.405.

Müller, D., U. Wandinger, D. Althausen, and M. Fiebig. 2001. "Comprehensive Particle Characterization from Three-Wavelength Raman-Lidar Observations: Case Study." *Applied Optics* 40 (27): 4863–4869. doi:10.1364/AO.40.004863.

Müller, D., U. Wandinger, and A. Ansmann. 1999. "Microphysical Particle Parameters from Extinction and Backscatter Lidar Data by Inversion with Regularization: Simulation." *Applied Optics* 38: 2358–2368. doi:10.1364/AO.38.002358.

Osterloh, L., C. Pérez, D. Böhme, J. M. Baldasano, C. Böckmann, L. Schneidenbach, and D. Vicente. 2009. "Parallel Software for Retrieval of Aerosol Distribution from LIDAR Data in the Framework of EARLINET-ASOS." *Computer Physics Communications* 180 (11): 2095–2102. doi:10.1016/j.cpc.2009.06.011.

Sasano, Y., and H. Nakane. 1984. "Significance of the Extinction/Backscatter Ratio and the Boundary Value Term in the Solution for the Two-Component Lidar Equation." *Applied Optics* 23: 11–13. doi:10.1364/AO.23.0011_1.

Strapp, J. W., W. R. Leaitch, and P. S. K. Liu. 1992. "Hydrated and Dried Aerosol-Size-Distribution Measurements from the Particle Measuring Systems FSSP-300 Probe and the Deiced PCASP-100x Probe." *Journal of Atmospheric and Oceanic Technology* 9: 548–555. doi:10.1175/1520-0426(1992)009<0548:HADASD>2.0.CO;2.

Takamura, T., Y. Sasano, and T. Hayasaka. 1994. "Tropospheric Aerosol Optical Properties Derived from LIdar, Sun Photometer, and Optical Particle Counter Measurements." *Applied Optics* 33 (30): 7132–7140. doi:10.1364/AO.33.007132.

Willeke, K., and P. A. Baron. 1993. *Aerosol Measurements Principles, Techniques and Applicatio*ns, 143–195. New York: Van Nostrand Reinhold.